A Linear Active Disturbance Rejection Control applied for DFIG based Wind Energy Conversion System

Ali Boukhriss[1], Tamou Nasser[2] and Ahmed Essadki [3]

[1] Laboratoire de Génie électrique, ENSET, Université Mohamed 5 Rabat, Morocco

[2] Ecole Nationale Suprieure d'Informatique et d'Analyse des Systemes, Université Mohamed 5 Rabat, Morocco

[3] Laboratoire de Génie électrique, ENSET, Université Mohamed 5 Rabat, Morocco

Abstract

This paper proposes the control of a doubly fed induction generator DFIG used in wind turbine energy conversion. The control strategy is based on the linear active disturbance rejection control ADRC to generate the control voltages of the rotor side converter RSC and the grid side converter GSC, due to the changes in control inputs. The ADRC, based on the extended state observer ESO, estimate and compensate in real time all the internal and external disturbance of the physical plant, such as, the parameter uncertainties due to the temperature variation, the cross-coupling terms and the load current variation into the dc link voltage. Simulations results are carried out with MATLAB /SIMULINK.

Keywords: *Doubly Fed Induction Generator, Active Disturbance Rejection Control, Extended State Observer, Wind Energy, Back To Back Converter.*

1. Introduction

Now the global trend towards the use of renewable energy is increasing, in this case, wind energy begins to take a large part in the global market. Variable speed wind using DFIG have a major advantage, seen mainly in reducing of the size and cost of power converters, in fact the power transiting through the back to back converter is about 30–40% of its rated power [1], while allowing a variation of the rotor speed over a range of 0.7 to 1.3 of the synchronous speed. The control of DFIG using PI controller is widely used [2][3], however it has a major drawback when the internal DFIG parameters are subject to variations due to the effects of temperature, which consequently affect the performance of regulators [4][5]. ADRC method proposes a control law which is not based on the accurate mathematical model of the system [6][7], therefore all internal and external disturbances are estimated and rejected in real time, hence the name of the active disturbance rejection control ADRC. In this paper, ADRC is used to control the rotor side converter RSC and the grid side converter GSC.

2. Dynamic Model

The model system of converting wind power using DFIG is represented in Fig.1. The kinetic energy of wind is converted by the turbine connected via a gear box to the axis of the DFIG. The stator is connected to the network through a back to back converter through the filter (R_f, L_f), while the stator is directly connected to the network. Vector control techniques are used for decoupling of active and reactive power. Unity power factor is often set at GSC and reactive power is transited directly between the network and the stator depending on the command of the RSC.

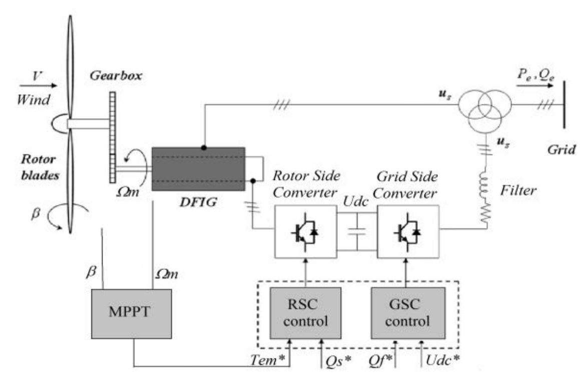

Fig. 1 Schematic diagram of DFIG-based wind generation systems.

In this paper three commands will be developed to ensure the functioning of the wind turbine: Maximum power point tracking control MPPT, control of rotor current at RSC and control of the DC link voltage and power factor at GSC.

IJCSI International Journal of Computer Science Issues, Vol. 10, Issue 2, No 2, March 2013
ISSN (Print): 1694-0814 | ISSN (Online): 1694-0784
www.IJCSI.org

3. Mathematical Model

3.1 Turbine Model

The power and the torque on the shaft of the turbine are given by the expression:

$$P_t = \frac{1}{2} C_p(\lambda, \beta) \rho S v^3 \tag{1}$$

$$T_t = \frac{1}{2} C_p(\lambda, \beta) \rho S \frac{v^3}{\Omega_t} \tag{2}$$

Where λ is the Tip speed ratio of the rotor blade tip speed to wind speed defined as:

$$\lambda = \frac{\Omega_t R}{v} \tag{3}$$

ρ is the air density, S is the surface swept by the blades of the turbine, Ω_t is the turbine speed, v the wind speed, β pitch angle and Cp represents the wind turbine power coefficient given by the empirical expression:

$$C_p(\lambda, \beta) = 0.22\left(\frac{116}{\lambda_i} - 0.4\beta - 5\right) e^{-\frac{12.5}{\lambda_i}} + 0.0068\lambda \tag{4}$$

$$\frac{1}{\lambda_i} = \frac{1}{\lambda + 0.08\beta} - \frac{0.035}{\beta^3 + 1} \tag{5}$$

Fig.2 shows the Cp curve for *β=0.*

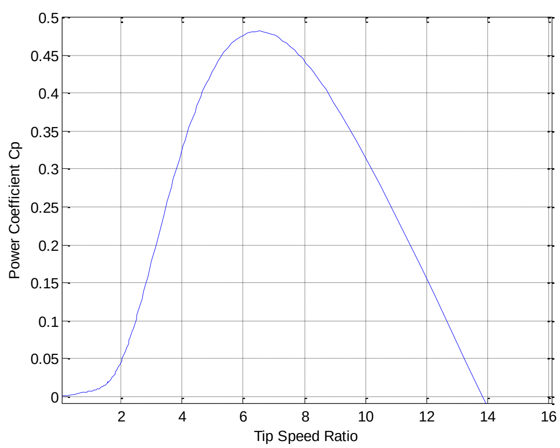

Fig. 2 Turbine power coefficient.

The turbine shaft is connected to that of the DFIG through a speed multiplier k. Fig.3 shows the mechanical model where J_t and J_m represent respectively the coefficient of inertia of the turbine and the generator and f_v is the viscosity coefficient. T_t and T_m represent respectively mechanical torque of turbine shaft and generator. Ω_m is the rotational speed of the generator. Mechanical equation is written as:

$$\left(\frac{J_t}{k^2} + J_m\right)\frac{d\Omega_m}{dt} + f_v \Omega_m = T_m - T_{em} \tag{6}$$

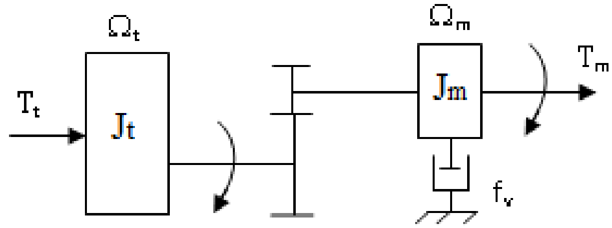

Fig. 3 Turbine model.

3.2 DFIG Model

The model of DFIG is established in the synchronous reference dq. Stator and rotor voltages are given by the following expressions, where R, L, L_m, and ϕ and I represent respectively resistance of windings, inductance, mutual inductance, flux and current. The subscripts s, r, d and q respectively indicate stator, rotor, d-axis and q-axis.

$$V_{ds} = R_s I_{ds} + \frac{d\phi_{ds}}{dt} - \dot{\theta}_s \phi_{qs} \tag{7}$$

$$V_{qs} = R_s I_{qs} + \frac{d\phi_{qs}}{dt} + \dot{\theta}_s \phi_{ds} \tag{8}$$

$$V_{dr} = R_r I_{dr} + \frac{d\phi_{dr}}{dt} - \dot{\theta}_r \phi_{qr} \tag{9}$$

$$V_{qr} = R_r I_{qr} + \frac{d\phi_{qr}}{dt} + \dot{\theta}_r \phi_{dr} \tag{10}$$

$$\phi_{ds} = (L_m + Ll_s) I_{ds} + L_m I_{dr} \tag{11}$$

$$\phi_{qs} = (L_m + Ll_s) I_{qs} + L_m I_{qr} \tag{12}$$

$$\phi_{dr} = (L_m + Ll_r) I_{dr} + L_m I_{ds} \tag{13}$$

$$\phi_{qr} = (L_m + Ll_r) I_{qr} + L_m I_{qs} \tag{14}$$

Electromagnetic torque Te is written as:

$$T_e = \frac{3}{2} p \frac{L_m}{L_m + Ll_s} (\phi_{qs} I_{dr} - \phi_{ds} I_{qr}) \tag{15}$$

Active and reactive stator power is given in synchronous reference dq-axis by the expression:

$$P_s = \frac{3}{2}(V_{ds} I_{ds} + V_{qs} I_{qs}) \tag{16}$$

$$Q_s = \frac{3}{2}(V_{qs} I_{ds} - V_{ds} I_{qs}) \tag{17}$$

3.3 **Back to Back PWM Modeling**

The back to back allows bidirectional transit of power between the rotor and the network [8]. Fig.4 represents the rectifier and inverter connected by the dc link voltage.

IJCSI
www.IJCSI.org

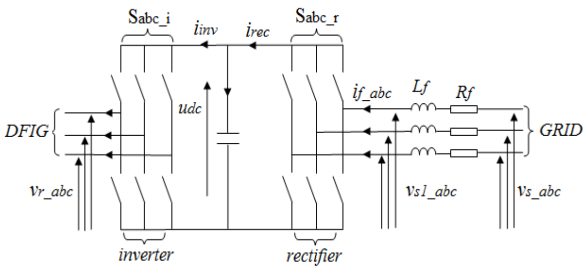

Fig. 4 back to back converter.

S_{mn} indicates switching functions corresponding to the IGBT switches where (m denotes a, b and c arms and n denotes inverter i or rectifier r). i_f , i_{rec} and i_{inv} are respectively the current in the filter, the output current of the rectifier and the input current of the inverter. i_{inv} is considered as a load current for the rectifier converter. In dq-axis reference frame, relations between voltage and current are given by:

$$C\frac{du_{dc}}{dt} = i_{rec} - i_{inv} \tag{18}$$

$$i_{rec} = \frac{3}{2}\left(S_{qr}I_{qf} + S_{dr}I_{df}\right) \tag{19}$$

$$L_f\frac{dI_{df}}{dt} + R_f I_{df} + L_f\omega_s I_{qf} = V_{ds} - V_{ds1} \tag{20}$$

$$L_f\frac{dI_{qf}}{dt} + R_f I_{qf} - L_f\omega_s I_{df} = V_{qs} - V_{qs1} \tag{21}$$

$$V_{ds1} = S_{dr}u_{dc} \tag{22}$$

$$V_{qs1} = S_{qr}u_{dc} \tag{23}$$

4. Active Disturbance Rejection Control

The active disturbance rejection control was proposed by Han [9][10][11][12]. It is designed to deal with systems having a large amount of uncertainty in both the internal dynamics and external disturbances. The particularity of the ADRC design is that the total disturbance is defined as an extended state of the system; and estimated using a state observer, known as the extended state observer (ESO). It was also simplified to linear ADRC using the linear ESO, which makes it easy and convenient to implement [13][14]. We consider the case of first order system for the illustration of the method.

$$\dot{y} = f(y,w,t) + b_0 u \tag{24}$$

Where u and y are input and output variables. w is the external disturbance, and $f(y,w,t)$ represents the combined effect of internal dynamics and external disturbance and b_0 parameter to estimate.

The basic idea is the estimation and compensation of f. Eq. (24) can be written in an augmented state space form as:

$$\begin{cases} \dot{x}_1 = x_2 + b_0 u \\ \dot{x}_2 = h \qquad where \qquad h = \dot{f} \\ y = x_1 \end{cases} \tag{25}$$

Or in the matrix form:

$$\begin{cases} \dot{x} = Ax + b_0 Bu + Eh \\ y = Cx \end{cases} \tag{26}$$

Where

$$A = \begin{bmatrix} 0 & 1 \\ 0 & 0 \end{bmatrix};\ B = \begin{bmatrix} 1 \\ 0 \end{bmatrix};\ C = \begin{bmatrix} 1 \\ 0 \end{bmatrix}^t;\ E = \begin{bmatrix} 0 \\ 1 \end{bmatrix}$$

A state observer of Eq. (25) will estimate the derivatives of y and f since Eq. (25) is now a state in the extended state model.

This observer denoted as a Linear Extended State Observer LESO is constructed as:

$$\begin{cases} \dot{z} = Az + b_0 Bu + L(y - \tilde{y}) \\ \tilde{y} = Cz \qquad where \qquad L = \begin{bmatrix} \beta_1 \\ \beta_2 \end{bmatrix} \end{cases} \tag{27}$$

L is the observer gain vector. To simplify the tuning process, the observer gains are parameterized as [15]:

$$L = \begin{bmatrix} 2\omega_0 \\ \omega_0^{\ 2} \end{bmatrix}$$

Where, ω_0 is the bandwidth of the observer determined by the pole placement technique [15]. The estimate is more precisely by increasing the bandwidth of the observer; however, a wide bandwidth increases the sensitivity to noise. In practice, a compromise is made between the speed at which the observer tracks the states and its sensitivity to sensor noise. With a properly designed ESO, z_1 and z_2 are tracking respectively y and f.

The control law is given by:

$$u = \frac{u_0 - z_2}{b_0} \tag{28}$$

The original plant in Eq. (24) is reducing to a unit gain integrator.

$$\dot{y} = (f - z_2) + u_0 \approx u_0 \tag{29}$$

This can be controlled by a simple proportional controller.

$$u_0 = k_p(r - z_1) \tag{30}$$

Where, r is the input signal reference to track.

The controller tuning is chosen as $k_p=\omega_c$, where ω_c is the desired closed loop frequency [14].

The combination of linear ESO and the controller is the linear ADRC. Generally we choose ω_0=3~7ω_c, and consequently, ω_c is the only tuning parameter. Fig.5 represents the implementation of the linear ADRC.

IJCSI International Journal of Computer Science Issues, Vol. 10, Issue 2, No 2, March 2013
ISSN (Print): 1694-0814 | ISSN (Online): 1694-0784
www.IJCSI.org

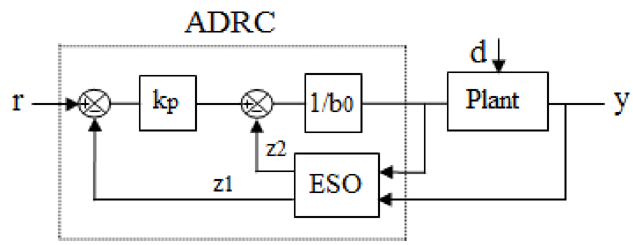

Fig. 5 Architecture of the developed ADRC controller.

5. Rotor Side Control

The control strategy is based on the orientation of the stator flux on the d-axis. We recall that the voltage of a stator phase in $\alpha\beta$ reference is given by:

$$\begin{cases} V_\alpha = R_s i_\alpha + \dfrac{d\phi_{\alpha s}}{dt} \\ V_\beta = R_s i_\beta + \dfrac{d\phi_{\beta s}}{dt} \end{cases} \tag{31}$$

Angle θ_s required to the Park transformation can be calculated as:

$$\begin{cases} \phi_{\alpha s} = \int (V_\alpha - R_s i_\alpha) dt \\ \phi_{\beta s} = \int (V_\beta - R_s i_\beta) dt \end{cases} \tag{32}$$

$$\theta_s = arctg\left(\frac{\phi_{\beta s}}{\phi_{\alpha s}}\right) \tag{33}$$

Neglecting the effect of the stator resistance R_s, it follows that the voltage and the stator flux are rotating at the same speed with a shift angle of 90°. It follows:

$$\begin{cases} V_{ds} \approx 0 \\ V_{qs} \approx V_s \end{cases} \tag{34}$$

The electromagnetic torque and the stator reactive power are given by:

$$T_e = -\frac{3}{2} p \frac{L_m}{L_s} \phi_{ds} I_{qr} \tag{35}$$

$$Q_s = \frac{3}{2} V_{qs} \left(\frac{\phi_{ds}}{L_s} - \frac{L_m}{L_s} I_{dr} \right) \tag{36}$$

$$where \quad \begin{cases} L_s = L_m + Ll_s \\ L_r = L_m + Ll_r \end{cases}$$

The electromagnetic torque T_e and reactive power Q_s are controlled respectively by the rotor currents I_{qr} and I_{dr}.
To get the electromagnetic torque reference T_{em}^{ref}, Maximum Power Point Tracking (MPPT) strategy is used to extract the maximum of power from the wind velocity. MPPT strategy applied in this paper only requires a rotation speed sensor. Maximum power extracted can be written as:

$$P_{t\max} = \frac{1}{2} C_{p\max} \rho \pi \frac{R^5}{\lambda_{opt}^{\ 3}} \Omega_t^{\ 3} \tag{37}$$

$$T_m = \frac{1}{2} C_{p\max} \rho \pi \frac{R^5}{k^2 \lambda_{opt}^{\ 3}} \Omega_m^{\ 2} \tag{38}$$

Where, λ_{opt} is the optimal tip speed ratio corresponding to maximum power coefficient C_{pmax}.
In a steady state and neglecting the effect of viscosity, Eq.(6) leads to $T_m = T_{em}$. It follows that the electromagnetic torque reference is given by:

$$T_{em}^{\ ref} = k_{opt} \Omega_m^{\ 2} \tag{39}$$

Where

$$k_{opt} = \frac{1}{2} C_{p\max} \rho \pi \frac{R^5}{k^2 \lambda_{opt}^{\ 3}} \tag{40}$$

The reference rotor currents are then deducted from Eqs.(35) and (36):

$$I_{dr}^{\ ref} = \frac{1}{L_m} \left(\phi_{ds} - \frac{2}{3} \frac{L_s}{V_{qs}} Q_s^{\ ref} \right) \tag{41}$$

$$I_{qr}^{\ ref} = -\frac{2}{3 p \phi_{ds}} \frac{L_s}{L_m} T_{em}^{\ ref} \tag{42}$$

The expressions of the rotor currents can be put into the form:

$$\frac{dI_{dr}}{dt} = \frac{V_{dr}}{\sigma L_r} - \frac{R_r}{\sigma L_r} I_{dr} + \omega_r I_{qr} + \omega_r \frac{L_m}{\sigma L_r L_s} \phi_{qs} - \frac{L_m}{\sigma L_r L_s} \frac{d\phi_{ds}}{dt} \tag{43}$$

$$\frac{dI_{qr}}{dt} = \frac{V_{qr}}{\sigma L_r} - \frac{R_r}{\sigma L_r} I_{qr} - \omega_r I_{dr} - \omega_r \frac{L_m}{\sigma L_r L_s} \phi_{ds} - \frac{L_m}{\sigma L_r L_s} \frac{d\phi_{qs}}{dt} \tag{44}$$

This, leads for the I_{dr} current, and the same study is used for I_{qr} current, to:

$$\frac{dI_{dr}}{dt} = f(I_{dr}, d, t) + b_0 u(t) \tag{45}$$

Where

$$\begin{cases} f = -\dfrac{R_r}{\sigma L_r} I_{dr} + \omega_r I_{qr} + \dfrac{L_m}{\sigma L_r L_s} \left(\omega_r \phi_{qs} - \dfrac{d\phi_{ds}}{dt} \right) + \left(\dfrac{1}{\sigma L_r} - b_0 \right) V_{dr} \\ u = V_{dr} \end{cases} \tag{46}$$

f represents the generalized disturbance, I_{dr} and u denote respectively the output and the control input of the plant, b_0 is the parameter gain to approximate. A linear active rejection control LADRC is easy to implement to control the rotor currents. Fig.6 shows a schematic block diagram for the rotor side control.

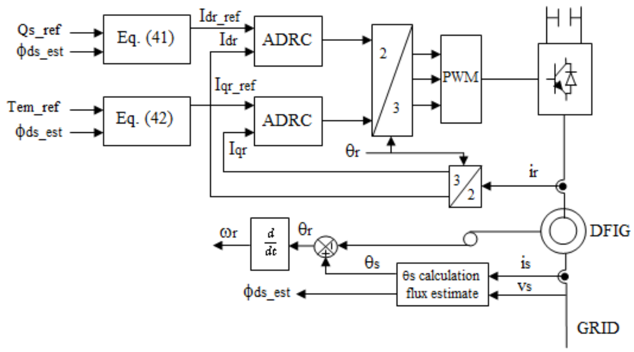

Fig. 6 schematic block diagram for the rotor side control.

6. Grid Side Control

This converter has two roles: to maintain the DC bus voltage constant regardless of the magnitude and direction of the rotor power flow and maintain a unity power factor at the connection point with the grid. A voltage oriented control VOC is used to control the grid side converter GSC.

6.1 Regulation of the Voltage Loop

If we neglected losses in three phase PWM rectifier, the input active power P_f is equal to the DC link power P_{dc}, that is:

$$P_f = P_{dc}$$

A phase locked loop PLL is used to orient the voltage on the q-axis and so the voltage on the d-axis is equal to zero. The input active P_f and reactive power Q_f is writing in dq-axis as:

$$P_f = \frac{3}{2}V_{qs}I_{qf} \quad (47)$$

$$Q_f = \frac{3}{2}V_{qs}I_{df} \quad (48)$$

$$P_{dc} = u_{dc}i_{rec} = \frac{3}{2}V_{qs}I_{qf} \quad (49)$$

Thus let to

$$cu_{dc}\frac{du_{dc}}{dt} = \frac{3}{2}V_{qs}I_{qf} - u_{dc}i_{inv} \quad (50)$$

Letting $w=u_{dc}^2$, then Eq. (50) can be expressed as:

$$\frac{dw}{dt} = \frac{3}{c}V_{qs}I_{qf} - \frac{2}{c}w^{1/2}i_{inv} \quad (51)$$

Eq. (51) can be written in the form:

$$\frac{dw}{dt} = f + b_0 u \quad (52)$$

Where

$$\begin{cases} f = -\frac{2}{c}w^{1/2}i_{inv} + \left(\frac{3}{c}V_{qs} - b_0\right)I_{qf} \\ u = I_{qf} \end{cases} \quad (53)$$

Where, f represents the generalized disturbance, w and I_{qf} are respectively the output and the control input of the plant. b_0 the parameter to approximate.
So the linear ADRC can be used in the voltage loop.

6.2 Regulation of the Current Loop

Eqs. (20) and (21) that represent the currents in the filter can be written as:

$$\frac{dI_{df}}{dt} = \frac{1}{L_f}\left(V_{ds} - R_f I_{df} - L_f\omega_s I_{qf}\right) - \frac{1}{L_f}V_{ds1} \quad (54)$$

$$\frac{dI_{qf}}{dt} = \frac{1}{L_f}\left(V_{qs} - R_f I_{qf} + L_f\omega_s I_{df}\right) - \frac{1}{L_f}V_{qs1} \quad (55)$$

This led to put the current I_{df}, and the same studies can be used for I_{qf}, into the form:

$$\frac{dI_{df}}{dt} = f\left(I_{df}, d, t\right) + b_0 u(t) \quad (56)$$

Where

$$\begin{cases} f = \frac{1}{L_f}\left(V_{ds} - R_f I_{df} - L_f\omega_s I_{qf}\right) - \left(\frac{1}{L_f} + b_0\right)V_{ds1} \\ u = V_{ds1} \end{cases} \quad (57)$$

As above a linear ADRC can be applied.

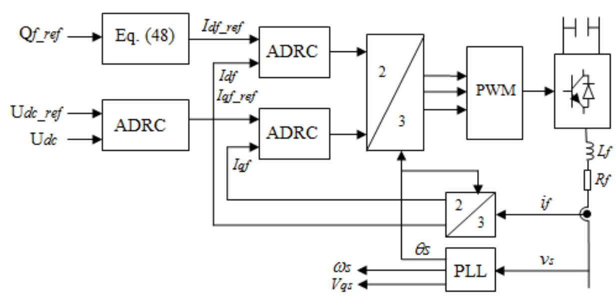

Fig. 7 schematic block diagram for the grid side control.

7. Simulation and Results

Simulation of the DFIG wind turbine and the applied control strategies have been carried out with the Matlab/Simulink. The parameters of the DFIG coupled to the turbine are given in Appendix. Simulations are made in three tests:

3.1 Test A

A constant wind speed $v=12m/s$ is applied to the turbine, which leads to a torque electromagnetic reference $T_{em}^{ref}=7911mN$ and a machine rotor speed equal to $n = 1740rpm$. A stator reactive power reference is set at 0 *MVAR*, which will be changed to $1MVAR$ at $t = 1s$ and then to 0 *Mvar* at $t = 1.5s$. Rotor currents I_{dr} and I_{qr} and their references I_{dr_ref} and I_{qr_ref} are plotted in Fig. 8. It is clear that the rotor currents follow well their references depending on response time imposed by the desired closed loop frequency $\omega_{cb}=60rd/s$ which correspond to $tr=50ms$.
Fig. 9 and Fig. 10 show the general disturbance f_I_{dr} and f_I_{qr} with their estimates by a linear ESO Z_2I_{dr} and Z_2I_{qr}; we can see that the ESO estimates in real time the total disturbances which will then be rejected by the linear ADRC. Rotor currents I_{dr} and I_{qr} and their estimates Z_1I_{dr} and Z_1I_{qr} are illustrated in Fig. 11; here also the ADRC puts again in evidence its performances. The decoupling effect between the direct and quadratic stator flux is illustrated in Fig. 12. Reactive stator power and their reference are shown in Fig. 13. The stator voltage v_s and the stator current i_s are in phase before $t = 1s$ and they are no longer in phase after $t = 1s$, indeed, the reactive power is a step change from 0 to $1MVAR$ as shown in Fig. 14.
Fig. 15 illustrates the regulation of DC bus voltage U_{dc}, which follows its reference after a transitional regime.

3.2 Test B

A second test is performed linearly varying wind speed from 10 m/s at $t=1s$ to $10.7m/s$ at $t=1.5s$. The corresponding rotor speed varies between $n=1450rpm$ (hypo synchronous mode) to $n=1550rpm$ (hyper synchronous mode) as shown in Fig. 16. Rotor power P_r transiting through the back to back converter is negative in hypo synchronous mode and positive in hyper synchronous mode indeed the slip changes the sign as illustrated in Fig. 17.

3.3 Test C

A third test is performed under the conditions of the first trial to reveal the robustness of the controller. Rotor resistance was varied by taking the values of $0.5Rr$, Rr and finally $1.4Rr$ to highlight the possible variations in the rotor resistance which can be due to a temperature rise. Fig. 18 demonstrates robust control based on linear active disturbance rejection control. The global uncertainties are estimated and compensated in real time.

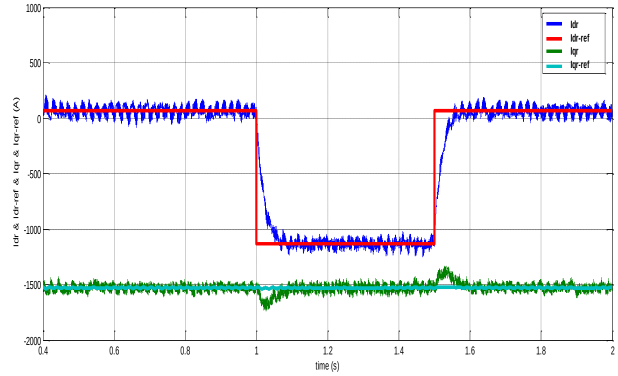

Fig. 8 rotor current I_{dr} & I_{qr} and their reference I_{dr_ref} & I_{qr_ref}.

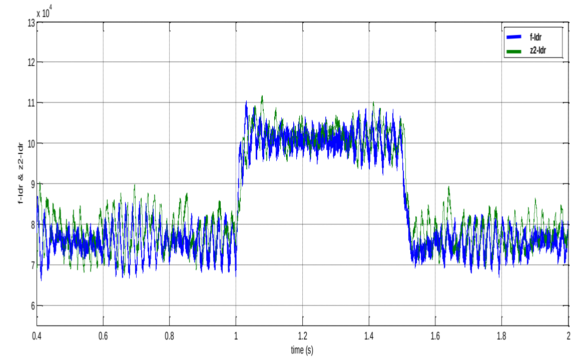

Fig. 9 general disturbance f_I_{dr} and their estimate z_2I_{dr}.

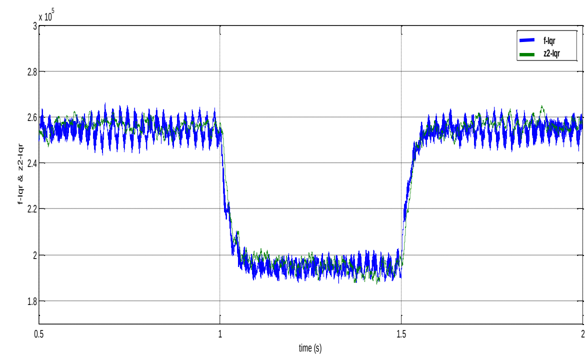

Fig. 10 general disturbance f_I_{qr} and their estimate z_2I_{qr}.

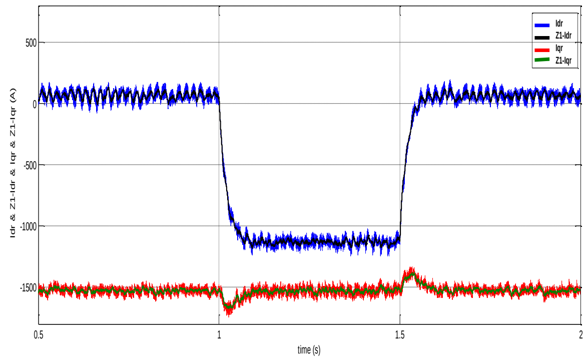

Fig. 11 rotor current I_{dr} & I_{qr} and their estimate z_1I_{dr} & z_1I_{qr}.

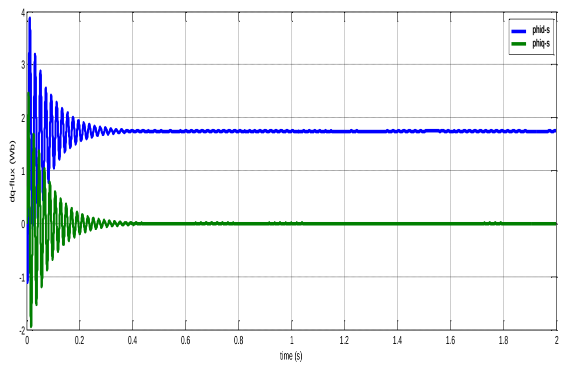

Fig. 12 direct and quadratic stator flux ϕ_{ds} & ϕ_{qs} .

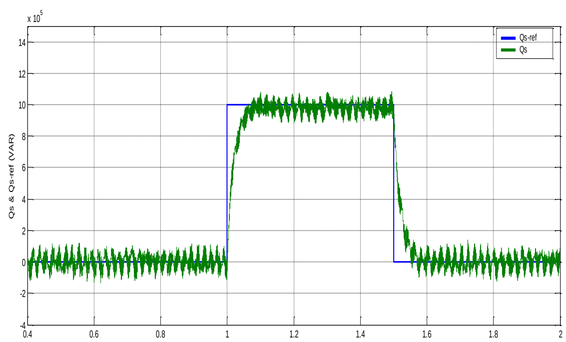

Fig. 13 stator reactive power Qs and their reference Qs_ref.

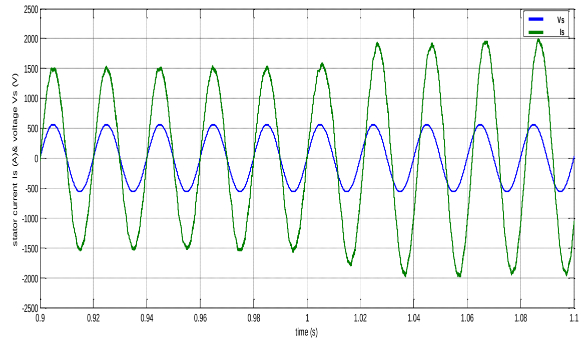

Fig. 14 stator voltage Vs and stator current Is.

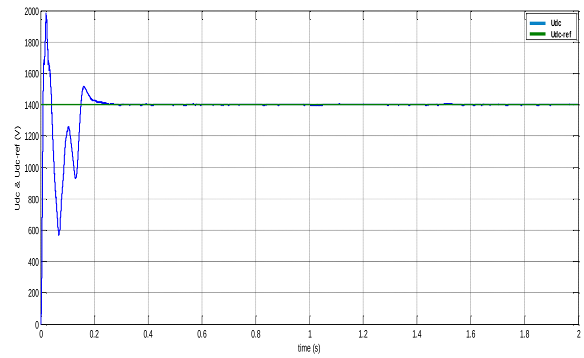

Fig. 15 DC link voltage Udc and Udc_ref.

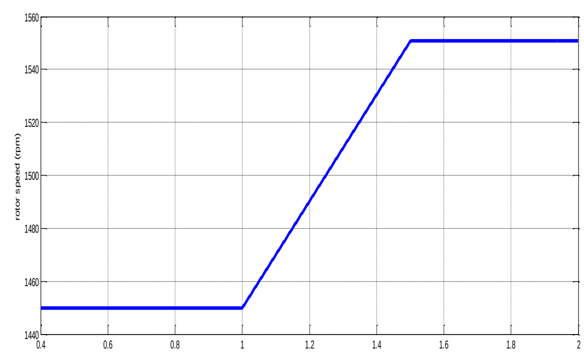

Fig. 16 rotor speed.

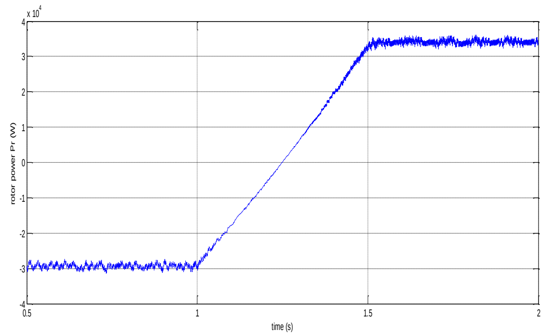

Fig. 17 rotor power P_r in hypo and hyper synchronous mode.

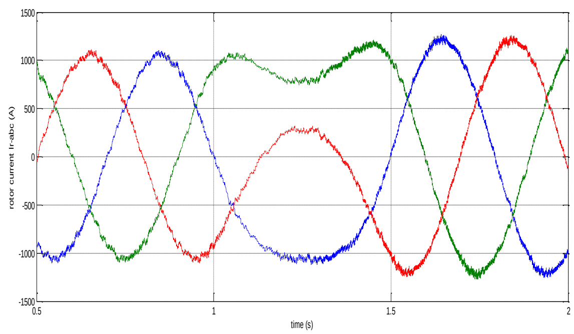

Fig. 18 instantaneous rotor current i_r .

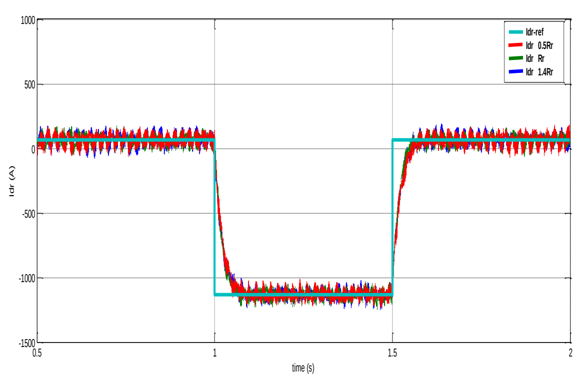

Fig. 19 rotor current I_{dr} for $0.5R_r$ - R_r - and $1.4R_r$ -

7. Conclusion

In this paper, we presented a new strategy for control of DFIG based wind energy system. The implementation of the ADRC based on linear ESO is easy to implement. It does not require exact knowledge of the internal dynamics of physical plant, which is the main reason that makes it robust against changes in internal parameters that affect the time constants of the DFIG current loops as in the traditional PI controller.

Appendix

Doubly fed induction generator parameters:

Rated power *1.5MW*
Grid voltage line to line rms $U=690V$ $f=50Hz$
Stator and rotor resistance $R_s=10.3m\Omega$ $R_r=8.28\ m\Omega$
Stator and rotor inductance $Ll_s=280.1\mu H$ $Ll_r=117.7\ \mu H$
Mutual inductance $L_m=26.96mH$
Number of pole pairs $p=2$

Turbine parameters

Rotor diameter $D=60m$
Total moment of inertia $J_t=303.96kgm^2$
Optimal tip speed ratio $\lambda_{opt}=6.5$
Maximal power coefficient $C_{pmax}=0.48$

DC link parameters

DC link voltage $U_{dc}=1400V$
Filter $L_f=0.25mH$ $R_f=0.785m\Omega$
DClink capacitor $C=50\ mF$

Rotor current controller parameters

Desired closed loop frequency $\omega_{cr}=60rd/s$
Observer bandwidth $\omega_{r0}=5\omega_{cr}=300rd/s$
Parameter gain $b_{r0}=2432$

Filter current controller parameters

Desired closed loop frequency $\omega_{cf}=300rd/s$
Observer bandwidth $\omega_{f0}=5\omega_{cf}=1500rd/s$
Parameter gain $b_{f0}=-4000$

Voltage loop parameters

Desired closed loop frequency $\omega_{cv}=30rd/s$
Observer bandwidth $\omega_{v0}=5\omega_{cv}=150rd/s$
Parameter gain $b_{v0}=33941$

References

[1] S. Heier, Grid Integration of Wind Energy Conversion Systems, 2nd edition, John Wiley & Sons, Chic ester, 2006.

[2] R. Pena, J. Clare and G. Asher, "A doubly fed induction generator using back-to-back PWM converters supplying an isolated load from a variable speed wind turbine" Electric Power Applications, IEE Proceedings, Vol. 143, 1996, pp.380-387.

[3] A. Boukhriss, A. Essadki and T. Nacer, "Power control for a doubly fed induction generator" Complex Systems (ICCS), 2012 International Conference on, 5-6 Nov. 2012.

[4] M. Comanescu, L. Xu and T.D. Batzel, "Decoupled current control of sensor less induction-motor drives by integral sliding mode" Industrial Electronics, IEEE Transactions on, Vol. 55, No. 11, October 2008,pp. 3836 – 3845.

[5] J. Hu and X. Yuan, "VSC-based direct torque and reactive power control of doubly fed induction generator", Renewable Energy, Vol. 40, 2012, pp. 13-23.

[6] Z. Gao, "Active disturbance rejection control: A paradigm shift in feedback control system design" Proc. of the American Control Conference, 2006, pp 2399-2405.

[7] L. Dong, P. Kandula, Z. Gao and D. Wang, "Active Disturbance Rejection Control for an Electric Power Assist Steering System", International Journal of Intelligent Control and Systems, Vol.15, No.1, March 2010, pp.18-24.

[8] R. Melicio, V.M.F. Mendes and J.P.S Catalao, "Comparative study of power converter topologies and control strategies for the harmonic performance of variable-speed wind turbine generator systems", Energy, Vol. 36, issue 1, January 2011, pp.520-529.

[9] J. Han, "Auto-disturbance rejection control and its applications", Control and Decision, Vol.13, No.1, 1998, pp. 19-23.

[10] J. Han, "From PID to auto disturbances rejection control", IEEE Transactions on Industrial Electronics, Vol. 56, No. 3, March 2009, pp.900-906.

[11] G. Tian and Z. Gao, "Frequency Response Analysis of Active Disturbance Rejection Based Control System", Control Applications IEEE International Conference on, 2007, pp. 1595-1599.

[12] Z. Gao, Y. Huang, and J. Han, "An alternative paradigm for control system design" Proceedings of IEEE conference on Decision and Control, Vol. 5, 2001, pp. 4578-4585.

[13] Q. Zheng, "On Active Disturbance Rejection Control: Stability Analysis and Applications in Disturbance Decoupling Control", Ph.D. thesis, Department of Electrical and Computer Engineering, Cleveland State University, Cleveland, USA, 2009.

[14] Q. Zheng, Z. Chen and Z. Gao "A practical approach to disturbance decoupling control", Control Engineering Practice, Vol. 17, No. 9, 2009, pp.1016-1025.

[15] Z. Gao "Scaling and Bandwidth-Parameterization Based Controller", Proceedings of the 2003 American Control Conference, 2003, Vol. 6, pp. 4989-4996.

Ali Boukhriss was born in Agadir, Morocco. He received a License degree from ENSET School, Mohamed 5 Souissi University Rabat, and a master degree from ENSA School, Ibn Zohr University Agadir in 2011. He is currently working toward the PhD degree in electrical engineering research at ENSET, Mohamed 5 Souissi University Rabat, Morocco.

Tamou NASSER is currently an Associate Professor (Professeur Assistant) at the communication networks department of National High School for Computer Science and Systems (ENSIAS), Mohamed V Souisssi University, Morocco, since 2009. She received her PhD degree in 2005 and her research MS degree, in 2000, respectively, all in electrical engineering from Mohammadia Engineering School (EMI), Morocco. Her research interests renewable energy, motor drives, power system, and Smart Grid. Doctor Tamou NASSER is a member of Al Jazari research group.

AHMED ESSADKI is currently a Professor and university research professor at the electrical engineering department of ENSET, Mohamed V Souisssi University, Morocco. In 2000, He received his PhD degree from Mohammadia Engineering School (EMI), (Morocco).From1990 to 1993, he pursued his Master program at UQTR University, Quebec Canada, respectively, all in electrical engineering. His current research interests include renewable energy, motor drives and power system. Doctor Ahmed ESSADKI is a member of RGE Lab in research group leader.